# Supporting Information

**Pulsed-current electrodeposition of vertically aligned $NiO_x$ films for stable perovskite solar cells**

Qifan Wang,[a] Qing Li,[a] Haonan Wang,[a] Yiheng Shi,[a] Yangyue Zhang,[a] Mengyao Song,[a] Haotian Wu,[a] Jian Lin,[a] Ruiyang Yin,[b]* Yu Hou[a]* and Shuang Yang[a]*

## Experimental Section/Methods

### Materials

Nickel(II) nitrate hexahydrate ($Ni(NO_3)_2 \cdot 6H_2O$, 99%) was purchased from Damas-beta. Lithium nitrate ($LiNO_3$, 99.9%) was purchased from Aladdin. Potassium Nitrate ($KNO_3$, ≥99%) was purchased from Sinopharm Chemical Reagent Co., Ltd. Methylammonium iodide (MAI), methylamine hydrochloride (MACl) and formamidinium iodide (FAI) were purchased from Greatcell Solar Materials. Lead iodide ($PbI_2$, 99.99%) and lead bromide ($PbBr_2$, 99.9%) were purchased from Energy Chemical. Lead(II) chloride ($PbCl_2$, 99.999%), cesium iodide (CsI, 99.9%) and dimethyl sulfoxide (DMSO, 99.9%) were purchased from Sigma-Aldrich. N,N-dimethylformamide (DMF, 99%) and chlorobenzene (CB, 99.5%) were purchased from Alfa Aesar. [2-(3,6-dimethyl-9H-carbazol-9-yl)ethyl]phosphonic acid (Me-4PACz, >99%) was purchased from Tokyo Chemical Industry. Ethanol (AR, 99.7%) was purchased from General-Reagent. [6,6]-phenyl-C61-butyric acid methyl ester ($PC_{61}BM$, 99.5%) and bathocuproine (BCP, 99%) were purchased from Nichem chemicals. Indium-tin oxide (ITO) substrates (8 Ω per square) were purchased from Nippon Sheet Glass.

### Preparation of $NiO_x$

**Spin-Coating of $NiO_x$:** Nickel(II) acetate tetrahydrate (1.5 mmol) was dissolved in 2-methoxyethanol (5 mL), followed by the addition of strontium chloride hexahydrate (0.075 mmol). The mixture was magnetically stirred continuously for 12 h and then left to stand, yielding a homogeneous green $NiO_x$ precursor solution.

**Electrodeposition of $NiO_x$:** A fresh electrolyte containing $Ni(NO_3)_2 \cdot 6H_2O$ (0.1 M), $KNO_3$ (0.05 M), and $LiNO_3$ (0.01 M) was prepared prior to each deposition. The addition of $K^+$ improved the solution conductivity, while $Li^+$ acted as an ionic dopant during electrodeposition.[1] The supporting electrolyte does not alter the characteristic morphology of $NiO_x$ and therefore does not affect device performance through morphological changes. The electrolyte was used immediately and not stored overnight. Patterned ITO glass substrates were cleaned with soap, acetone, and ethanol under ultrasonication and then treated with ultraviolet ozone for 30 min. The ITO substrate was promptly mounted onto the platinum working electrode clamp. Deposition was performed using a electrochemical workstation with a standard three-electrode setup, employing an Ag/AgCl reference electrode and a Pt ring counter electrode. The electrolyte flow was maintained uniformly throughout, with the working electrode substrate perpendicular to the controlled fluid direction. Variations in $T_{on}$ and $T_{off}$ affected the peak potential during pulsed deposition. To prevent film quality degradation caused by excessively low instantaneous potential, the current density for CCED was set to 0.5 mA $cm^{-2}$. The pulse current density was adjusted under the condition that the potential window remained consistent with that of CCED. A pulse on-time of 300 ms was used. Better film quality was achieved when the duty cycle ranged from 30% to 40%, and most of the pulse duty cycles used in this experiment were set to 40%. Deposition was terminated when the charge reached 20 mC $cm^{-2}$. Notably, before film growth, the electrolyte was purged with nitrogen for 15 min, and a gentle nitrogen flow was sustained during deposition. Nitrogen saturation minimizes side reactions and ensures a chemically stable deposition environment. After deposition, the sample was immediately removed, rinsed thoroughly with deionized water, and dried under a nitrogen stream.

**Annealing**: The Nickel oxide precursor film samples were transferred to a muffle furnace and annealed at 250 °C for 15 min and then at 300 °C for 60 min. After natural cooling, the ITO/$NiO_x$ samples were obtained.

## Device fabrication

PSCs were fabricated with a p-i-n heterojunction configuration of ITO/$NiO_x$/Me-4PACz/perovskite/$PC_{61}BM$/BCP/Ag. ITO/$NiO_x$ substrates (prepared by electrodeposition or spin-coating) were coated with a Me-4PACz ethanol solution (0.5 mg $mL^{-1}$) via spin-coating at 4000 rpm for 30 s, followed by annealing at 100 °C for 10 min to form the SAM layer. For the composition $Cs_{0.05}FA_{0.85}MA_{0.1}PbI_3$, a perovskite precursor solution (1.5M) was prepared by mixing CsI, MAI, FAI and $PbI_2$ in DMF:DMSO=4:1, v/v mixed solvent subject to the

stoichiometric ratio. An additional 5 mol% $PbCl_2$ and 12.5 mol% MACl were added to the precursor for better crystallization and perovskite phase transformation. The perovskite film was spin-coated at 1000 rpm for 5 s and 5000 rpm for 40 s. At 5 s before the end of the second step, chlorobenzene (200 μL) was rapidly dripped onto the spinning substrate, followed by annealing at 100 °C for 30 min. Subsequently, A $PC_{61}BM$ layer (20 mg $mL^{-1}$ in chlorobenzene) was spin-coated at 2000 rpm for 50 s, followed by deposition of a BCP layer (0.5 mg $mL^{-1}$ in IPA) at 5000 rpm for 50 s, with the latter dispensed dynamically at full speed. Finally, a 100 nm thick Ag back electrode was thermally evaporated.

**Characterization**

The morphology of $NiO_x$ and perovskite films were characterized by field-emission SEM (HITACHI S4800). Field emission scanning electron microscopy (FESEM) and Focused Ion Beam (FIB) characterization were performed using ThermoFisher Helios G4 UC. FESEM images were recorded at 2 kV and 0.1 nA. Energy dispersive X-ray spectroscopy (EDS) was carried out using Oxford X-Max$^N$ (80 $mm^2$) at 15 kV, 0.4 nA. TEM sample preparation was carried out using FIB preparation technique with a 30 kV Ga-ion beam. The sample was thinned down to about 100 nm. Transmission electron microscopy (TEM) and Scanning transmission electron microscopy (STEM) characterization were performed using ThermoFisher Talos F200X (FETEM, 200 kV). High angle annular dark field (HAADF)-STEM images were recorded using a convergence semi angle of 11 mrad, and inner- and outer collection angles of 59 and 200 mrad, respectively. Energy dispersive X-ray spectroscopy (EDS) was carried out using 4 in-column Super-X detectors. All electrodeposition curves, as well as CV and LSV measurements, were conducted using a CHI660F electrochemical workstation. Atomic force microscopy (AFM, Bruker Dimension Icon) was used to characterize the morphology and potential distribution of the perovskite films. The wettability of DMF solvent on different substrates was measured under ambient conditions using a Dataphysics OCA20 contact-angle system. XRD patterns were obtained by Powder X-ray diffractometer (Bruker Advance D8, Cu Kα radiation, 40 kV). PL mapping was measured at room temperature using a laser-scanning fluorescence lifetime/intensity imaging system (FLRM300, Time-Tech Spectra, LLC) equipped with a 405 nm picosecond pulsed diode laser as an excitation source. Time-resolved photoluminescence (TRPL) spectra of perovskite films were acquired by Endinburgh FLS890 spectrometer under ambient conditions. And all PL measurements were tested based on unencapsulated films in air. Transmission spectra of $NiO_x$ and absorption spectra of CsFAMA perovskite films were measured using a Cary 500 UV-Vis-NIR spectrophotometer. The X-ray

photoelectron spectroscopy (XPS) was acquired with a ESCALAB QXi spectrometer. Nano-scratch tests under optical microscopy were performed using a Kla imicro instrument. The adhesion of perovskite films was tested using an E42.503 tensile testing machine. Perovskite adhesion tests were performed by scribing patterns using a compact thin-film laser etcher (YLET1010MG).

Electrochemical impedance spectra were measured out using an electrochemical workstation (CHI660F) in the frequency range of 1.0 MHz and 1.0 Hz at 0.5 V under dark conditions. Transient photocurrent/photovoltage decays (TPC/TPV) curves of solar cells were measured by digital storage oscilloscope (KEYSIGHT, DSOX3104T) under the excitation of pulsed laser (532 nm, DPS-532-A, 1 mJ) under an AM 1.5G light simulator (Solar IV-150A, Zolix). *J-V* curves of solar cells were measured under an AM 1.5G light simulator (Solar IV-150A, Zolix) calibrated to 100 mW $cm^{-2}$ by a standard KG5-filtered Si reference cell. All devices were measured by a Keithley 2400 digital source meter with a scan rate of 0.15 V $s^{-1}$. The device active area was masked to be 0.0625 $cm^2$. *I-V* curves were measured by applying a voltage signal through a Keithley 2400 digital source meter after depositing longitudinal electrodes on both the $NiO_x$ side and the ITO side. Steady state photocurrent output of the best-performing devices was measured by biasing the device at maximum power point for 500 s. External quantum efficiency (EQE) spectra of PSCs were acquired by Newport-74125 system. Mott-Schottky plots, thermal admittance spectroscopy (TAS), and drive-level capacitance profiling (DLCP) data were obtained using an LCR meter (Agilent E4980A). Long-term stability of the devices was measured under continuous one-sun illumination by adopting the device structure of ITO/$NiO_x$/Me-4PACz/perovskite/$PC_{61}BM$/BCP/Au.

**Mechanical Testing**

Mechanical test specimens were prepared in a symmetric sandwich structure. First, a thin layer of poly(methyl methacrylate) was spin-coated onto CsFAMA to protect the perovskite from chemical corrosion and surface strain caused by the epoxy adhesive. Next, 6 × 6 arrays of 4 $mm^2$ square patterns were laser-scribed onto the ITO glass using a compact thin-film laser etcher. Epoxy was applied onto the scribed CsFAMA, and an ITO glass cover was placed on top. The sample was then left in a glovebox at room temperature for 24 hours to cure the polymer. Finally, the top ITO cover was peeled off, leaving firmly adhered portions of the CsMAFA on the substrate. Overall, the PCED film exhibited a more complete retained area compared to the control.

Nano-scratch tests were performed using a diamond conical indenter with a tip radius of 5 μm and a cone angle of 90°. The procedure consisted of three steps: first, a pre-scan was conducted under a constant contact load of 10 μN along the scratch path to obtain the surface profile and tilt angle; second, the scratch load was linearly ramped to a preset maximum value; finally, a post-scan was performed under the same 10 μN contact load along the groove to measure the residual depth after load removal.

## Supplementary Notes

### Note S1. TRPL measurement

The double exponential equation is employed to model the decay curve in order to fit the TRPL results, represented by the following equation:

$$f(t) = A_1 exp^{(-\frac{t}{\tau_1})} + A_2 exp^{(-\frac{t}{\tau_2})} + B$$

Where, $\tau_1$ is the average lifetime of the fast decay process, $\tau_2$ is the average lifetime of the slow decay process,[2] $A_1$ and $A_2$ are constants representing the contribution rates of the fast and slow components,[3] and B is the constant for baseline offset.

### Note S2. SCLC measurement

The trap density can be determined by equation:[4]

$$N_{trap} = \frac{2\varepsilon_0 \varepsilon_r V_{TFL}}{eL^2}$$

Where, $\varepsilon_0$ is the relative dielectric constant of perovskite, $\varepsilon_r$ is the vacuum dielectric constant, $V_{TFL}$ is the trap filled limit voltage, e is the elementary charge, and L is the thickness of the active layer.

## Supplementary Figures

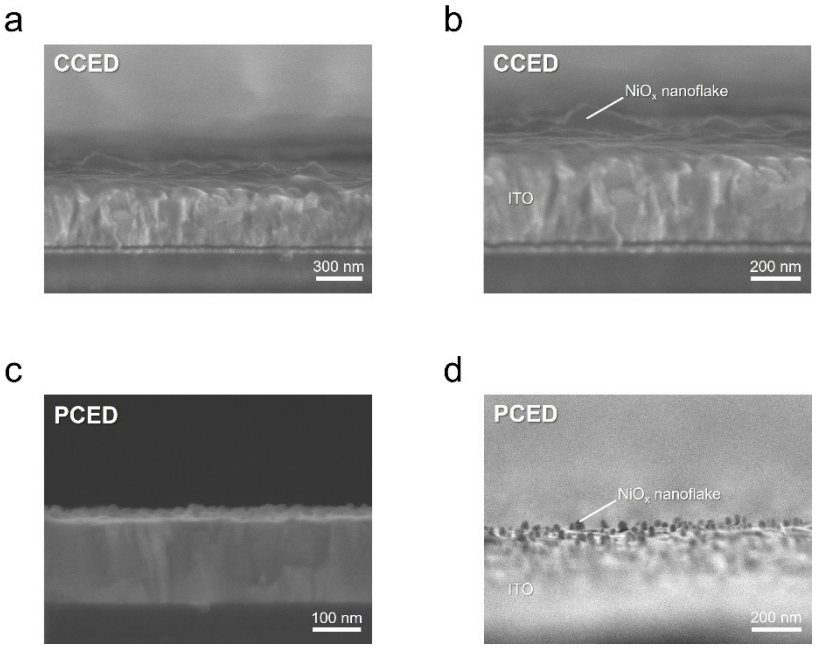


**Fig. S1** SEM images of (a, b) CCED-$NiO_x$ and (c, d) PCED-$NiO_x$.

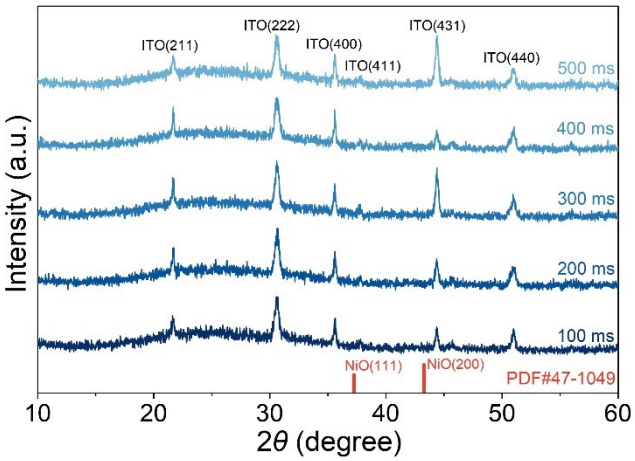


**Fig. S2** XRD patterns of $NiO_x$ prepared under different pulse $T_{on}$ conditions.

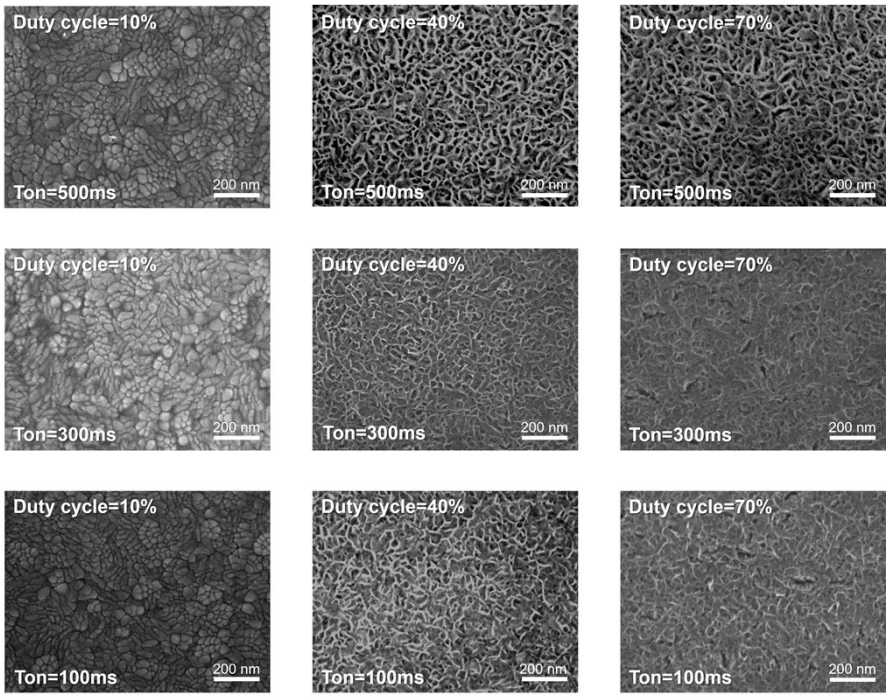


**Fig. S3** SEM images of $NiO_x$ synthesized under various pulse $T_{on}$ times and duty cycles.

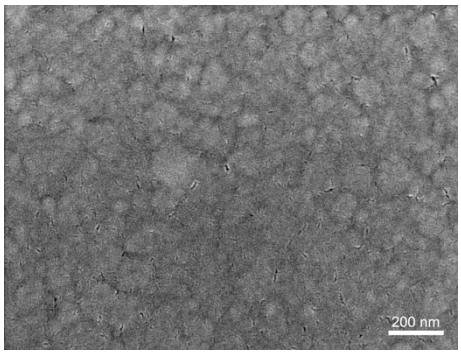


**Fig. S4** SEM morphology of the control $NiO_x$ sample deposited via liquid-phase spin-coating.

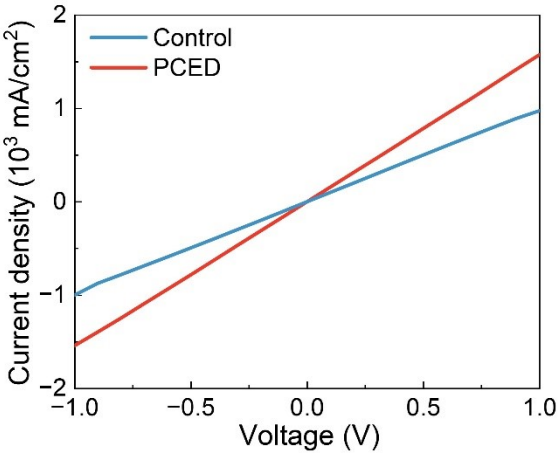


**Fig. S5** Electrical conductivity of control-$NiO_x$ and PCED-$NiO_x$ thin films.

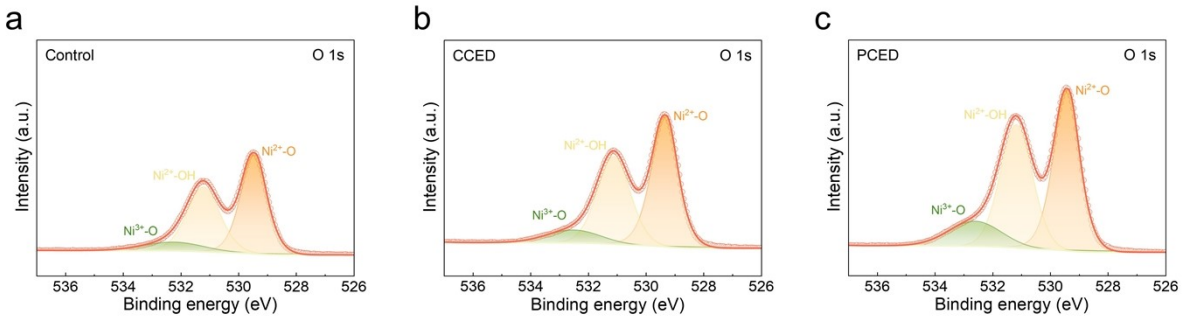


**Fig. S6** O 1s XPS spectra of (a) control-$NiO_x$, (b) CCED-$NiO_x$, and (c) PCED-$NiO_x$.

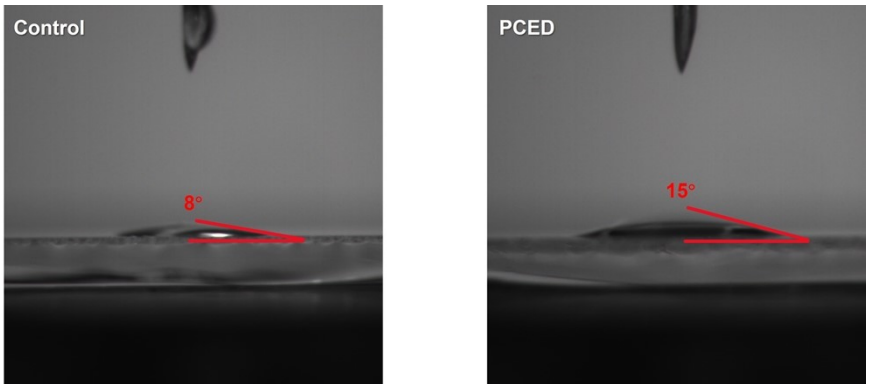


**Fig. S7** Contact angles of DMF solvent on various HTL surfaces.

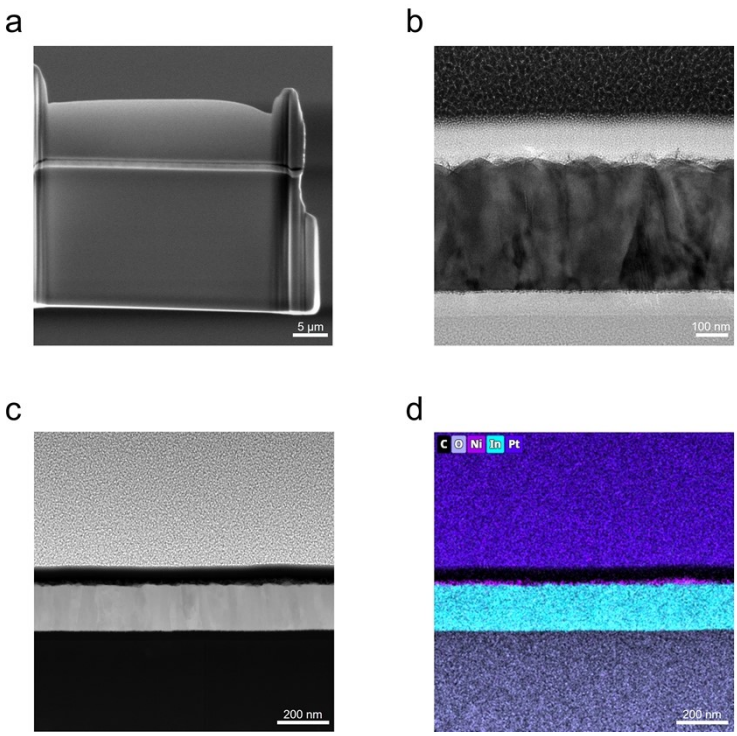


**Fig. S8** (a) TEM image and (b) enlarged view of the $NiO_x$ cross-section obtained via FIB. (c) HAADF image and (d) corresponding EDS mapping of the $NiO_x$ cross-section.

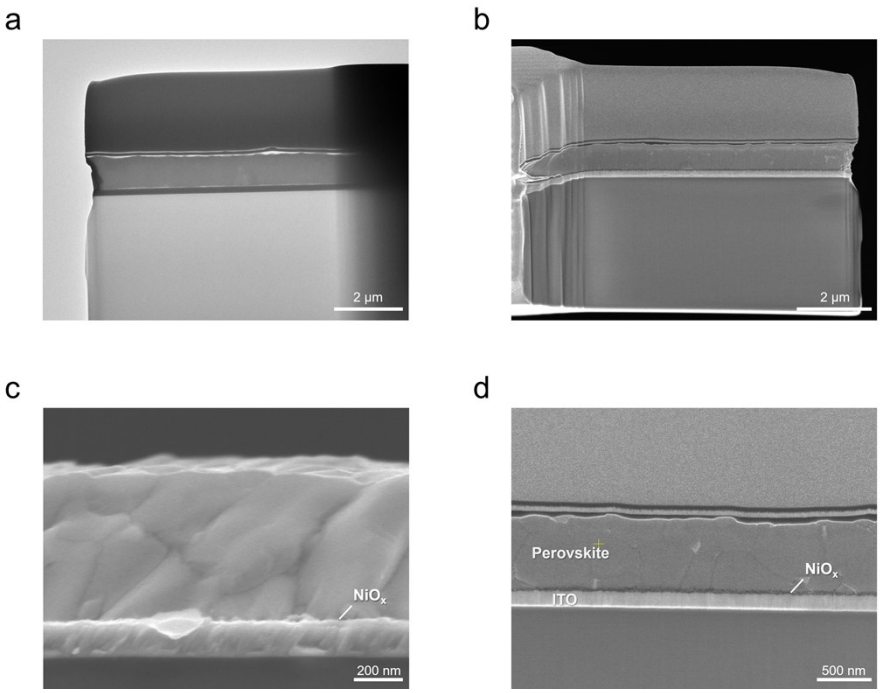


**Fig. S9** (a) TEM and (b) SEM images of the perovskite device cross-section prepared by FIB. (c-d) SEM images of the perovskite/$NiO_x$ heterointerface.

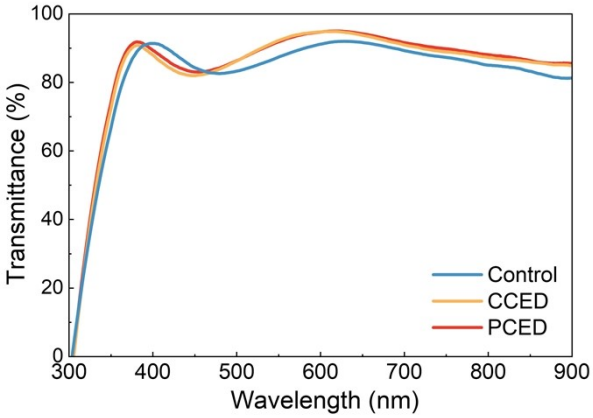


**Fig. S10** Transmittance spectra of $NiO_x$ layers on ITO/glass substrates prepared under different deposition conditions.

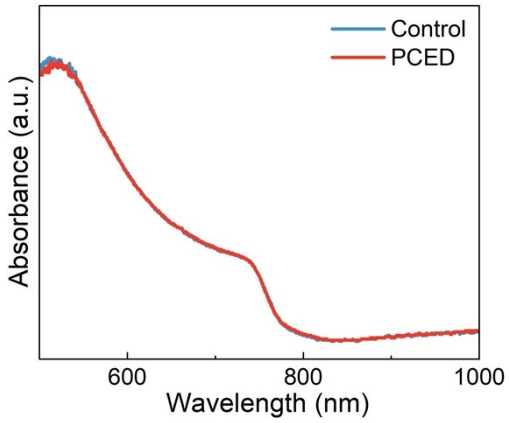


**Fig. S11** UV-Vis absorption spectra of the perovskite film.


**Fig. S12** PL intensity heatmaps of perovskite films deposited on control-$NiO_x$, CCED-$NiO_x$, and PCED-$NiO_x$ substrates, with 36 samples per batch from multiple preparation runs.

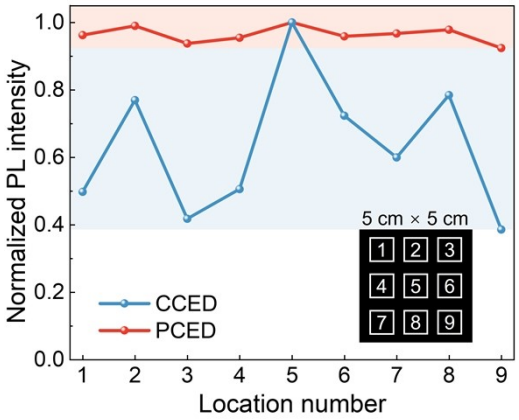


**Fig. S13** Normalized PL intensity of 5 × 5 $cm^2$ perovskite films when measured at different positions.

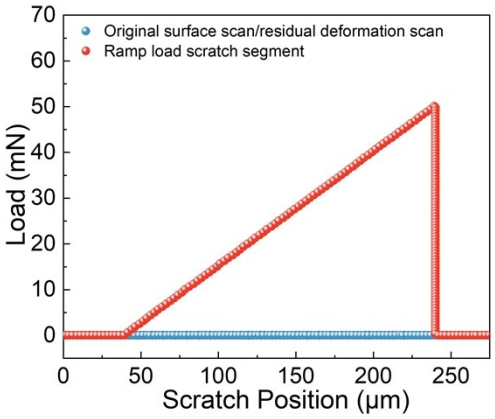


**Fig. S14** Plot of applied load versus scratch position for nano-indentation scratch, linear ramp-load scratch, and residual scratch.

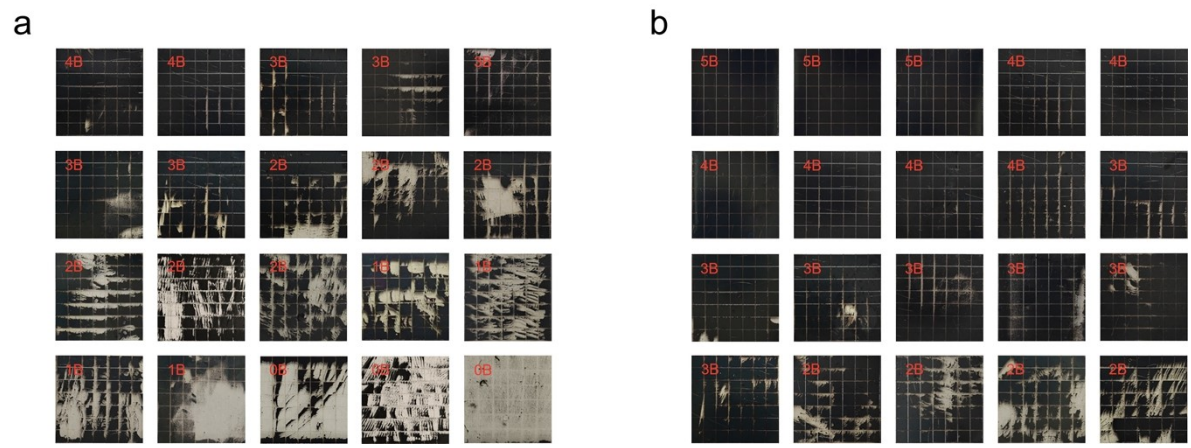


**Fig. S15** 20 adhesion test images of cross-sectioned perovskite regions on (a) control-$NiO_x$ and (b) PCED-$NiO_x$ substrates.

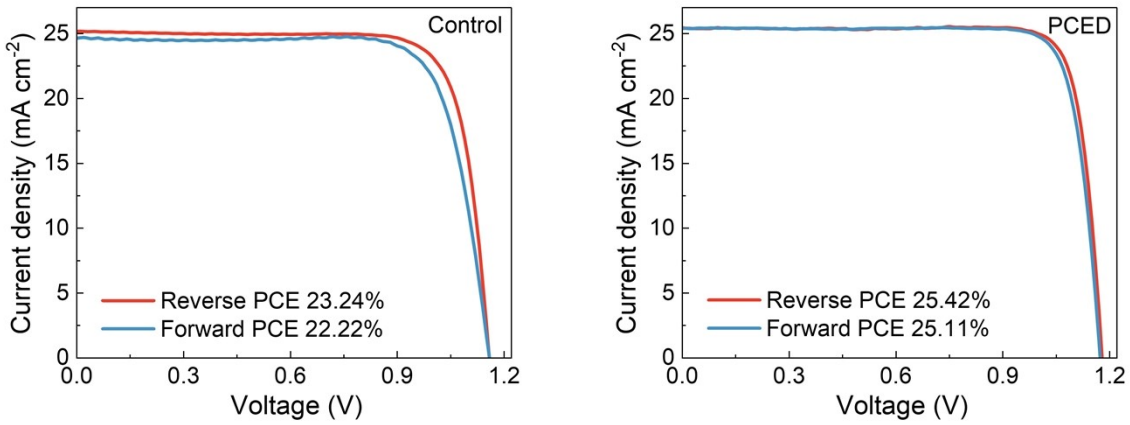


**Fig. S16** *J-V* characteristics of perovskite solar cells with different HTLs under forward and reverse scan directions.

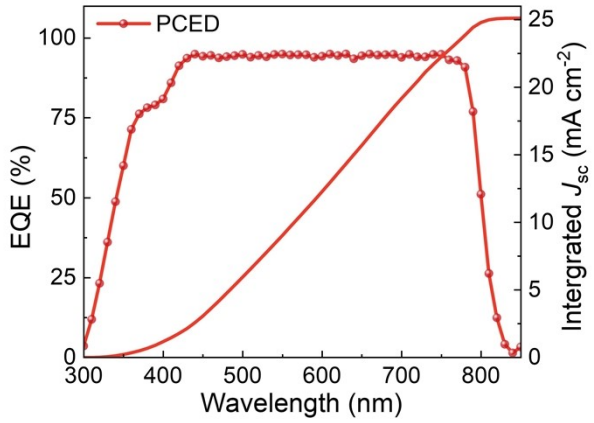


**Fig. S17** EQE spectra of PCED-$NiO_x$ devices.

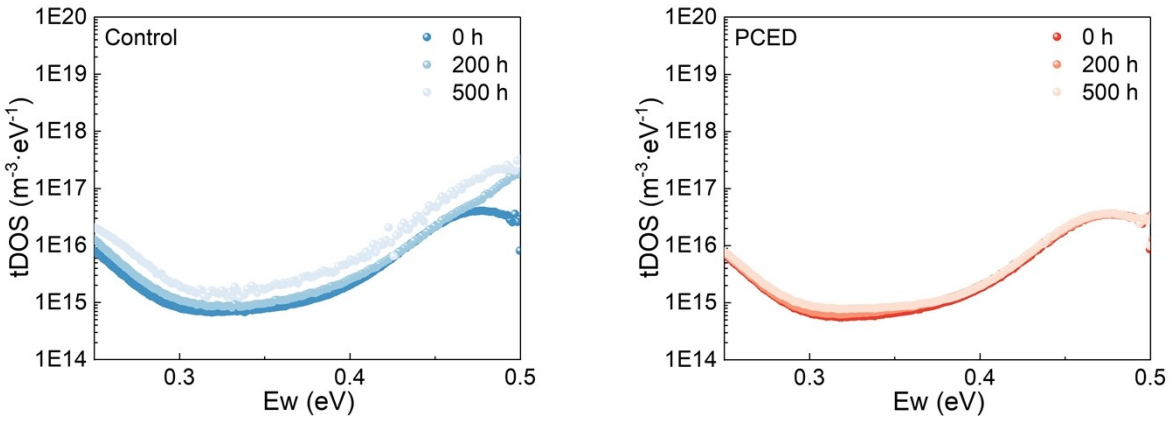


**Fig. S18** Trap density measurements of solar cells based on control-$NiO_x$ and PCED-$NiO_x$, stored under 1-sun illumination at 85 °C.

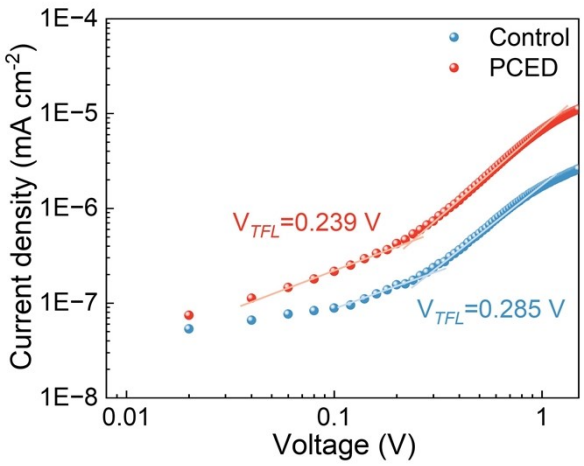


**Fig. S19** Dark *J-V* curves of the hole-only device based on the SCLC model.

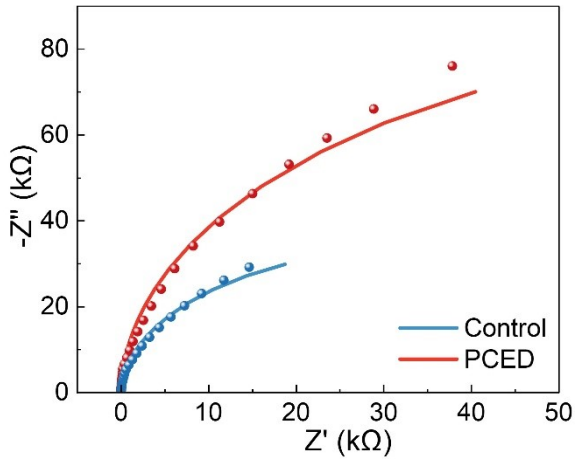


**Fig. S20** Nyquist plots of control-$NiO_x$ and PCED-$NiO_x$ based PSCs recorded at 0.5 V in dark condition.

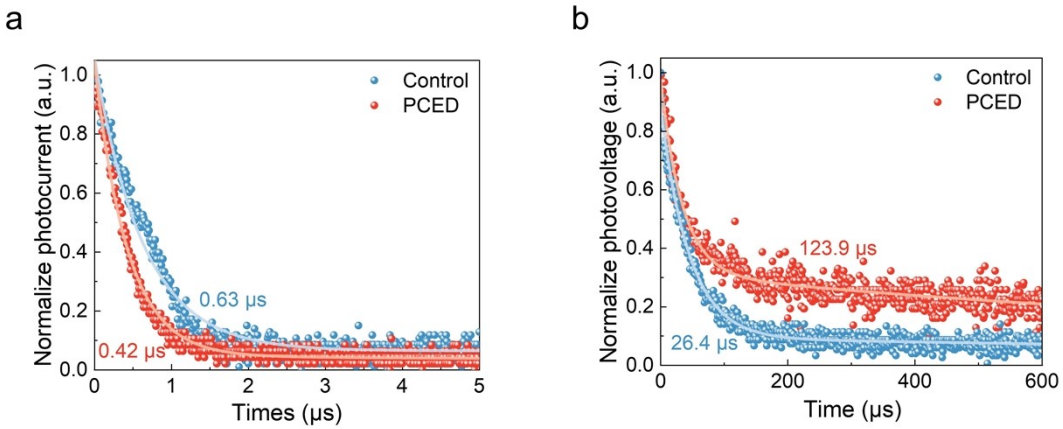


**Fig. S21** (a) TPC and (b) TPV curves of the control-$NiO_x$ and PCED-$NiO_x$ based PSCs.

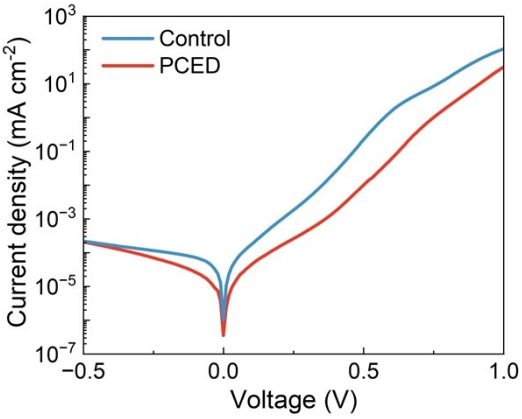


**Fig. S22** Dark current curves of solar cell devices based on control-$NiO_x$ and PCED-$NiO_x$.

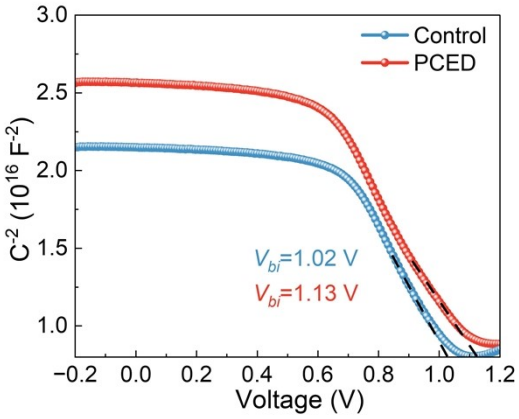


**Fig. S23** Mott-Schottky plots of perovskite solar cells based on control-$NiO_x$ and PCED-$NiO_x$ measured at 1 MHz.

## Supplementary Tables

**Table S1**. Lifetimes of perovskite films estimated by fitting TRPL curves with double-exponential model from the bottom (ITO) surface.

| Sample | $A_1$ | $\tau_1$ (ns) | $A_2$ | $\tau_2$ (ns) |
|---|---|---|---|---|
| Control | 0.77 | 12.88 | 0.17 | 75.21 |
| CCED | 0.42 | 6.57 | 0.57 | 32.80 |
| PCED | 0.73 | 3.14 | 0.21 | 29.33 |

**Table S2**. Correlation data between scratch depth profiles and maximum actual loads in three-cycle scratch tests.

| Control | Max load actual (mN) | Maximum depth (nm) | Residual depth (nm) | Elastic recovery (nm) |
|---|---|---|---|---|
| Scratch-1 | 50.08 | −502.455 | −80.062 | 422.393 |
| Scratch-2 | 50.11 | −514.717 | −109.616 | 405.101 |
| Scratch-3 | 50.08 | −526.971 | −118.269 | 408.702 |
| Average | 50.090 | −514.714 | −102.649 | 412.065 |

| PCED | Max load actual (mN) | Maximum depth (nm) | Residual depth (nm) | Elastic recovery (nm) |
|---|---|---|---|---|
| Scratch-1 | 50.09 | −530.338 | −105.694 | 424.644 |
| Scratch-2 | 50.08 | −527.711 | −114.716 | 412.995 |
| Scratch-3 | 50.11 | −537.987 | −113.909 | 424.078 |
| Average | 50.093 | −532.012 | −111.440 | 420.572 |

**Table S3**. Classification of delamination test results in ASTM D3359.[5,6]

| ASTM Classification | Description |
|---|---|
| 5B | Smooth edges; no squares detached. |
| 4B | Flakes detached at intersections, <5% area affected. |
| 3B | Flaked edges, 5%-15% area affected. |
| 2B | Flaked edges, ribbons or squares detached, 15%-35% area affected. |
| 1B | Flaked edges, ribbons or squares detached, 35%-65% area affected. |
| 0B | Any flaking not classified in above categories. |

**Table S4.** Photovoltaic parameters of PSCs measured under simulated AM 1.5G solar irradiation.

| | $V_{OC}$ (V) | $J_{SC}$ (mA cm$^{-2}$) | FF (%) | PCE (%) |
|---|---|---|---|---|
| Control | 1.16 | 25.21 | 79.60 | 23.24 |
| PCED | 1.18 | 25.51 | 84.54 | 25.42 |

**Table S5.** Comparison of recently reported photovoltaic parameters for $NiO_x$-based PSCs.

| Retained efficiency | Condition | Reference |
|---|---|---|
| **96.5%** | **Encapsulated, 1 sun illumination, 85 °C, 2130 h** | **This work** |
| >90% | Encapsulated, 1 sun illumination, 65 °C, 1200 h | *Science* **2023,** *382*, 284-289 |
| 85.4% | Encapsulated, 1 sun illumination, 50 °C, 1250 h | *Science* **2023,** *382*, 1399-1404 |
| 93.8% | $N_2$, 1 sun illumination, 85 °C, 1300 h | *Joule* **2025**, *9*, 101815 |
| >80% | $N_2$, 1 sun illumination, 85 °C, 800 h | *Energy Environ. Sci.* **2025**,*18*, 3235-3247 |
| >95% | Encapsulated, $N_2$, 1 sun illumination, 50 % RH, 60 °C, 700 h | *Energy Environ. Sci.* **2025**,*18*, 5424-5436 |
| 97% | Encapsulated, 1 sun illumination, 65 °C, 60% RH, 1500 h | *Adv. Mater.* **2025**, *37*, e07730 |
| 97.5% | Encapsulated, 1sun illumination, 1000 h | *Adv. Mater.* **2025**, *37*, e10553 |
| >87% | 1 sun illumination, Room temperature, 1000 h | *Adv. Mater.* **2025**, *37*, 2505087 |
| 90% | 1 sun illumination, 23±4 °C, 50% RH, 1500 h | *Adv. Mater.* **2025**, *37*, 2502865 |
| 95.4% | Encapsulated, 1 sun illumination, 65 °C, 1960 h | *Adv. Mater.* **2024**, *36*, 2303869 |

# References


[1] C. Tang, X. Ning, J. Li, H.-L. Guo and Y. Yang, *J. Mater. Sci. Technol.*, 2019, **35**, 1570–1577.

[2] X. Zhao, L. Tian, T. Liu, et al., *Journal of Materials Chemistry A* 2019, **7**, 1509.

[3] T. Yang, C. Ma, W. Cai, et al., *Joule* 2023, **7**, 574.

[4] Q. Dong, Y. Fang, Y. Shao, et al., *Science* 2015, **347**, 967.

[5] T. Duan, S. You, M. Chen, W. Yu, Y. Li, P. Guo, *Science* 2024, **384**, 878–884.

[6] T. Xiao, M. Hao, T. Duan, Y. Li, Y. Zhang, P. Guo, *Nature Energy* 2024, **9**, 999–1010.